Coupling Interactions of Distal Residues Enhance Dihydrofolate Reductase Catalysis: Mutational Effects on Hydride Transfer Rates†

P. T. Ravi Rajagopalan, Stefan Lutz,‡ and Stephen J. Benkovic*

Department of Chemistry, The Pennsylvania State University, University Park, Pennsylvania 16802

Received June 27, 2002; Revised Manuscript Received August 29, 2002

ABSTRACT: Recently, the participation in catalysis of residues spatially removed from the enzyme's active site has received considerable attention. The influence of the distal Gly-121 residue on the chemical step of hydride transfer in dihydrofolate reductase (DHFR) catalysis had been demonstrated previously [Cameron, C. E., and Benkovic, S. J. (1997) *Biochemistry 36*, 15792−15800]. In our continuing effort to identify catalytically important residues that are distal from the active site, we used sequence conservation information, kinetic data on site-directed mutants, dynamic motion information from NMR methods, and correlated motions from MD simulations to identify a subset of residues. Among them, the region spanning positions 41−45 is distal to the active site and was chosen as the focus for the mutagenesis and kinetic studies reported here. Specifically, the highly conserved Met-42 was selected for site-directed mutagenesis. While the reaction kinetics for the M42F mutant enzyme did not deviate from wild-type behavior, a 41-fold reduction in the forward hydride transfer rate was found for the M42W mutant. Given the established role of Gly-121 in the hydride transfer process, double mutant enzymes involving positions 42 and 121 were constructed and characterized. These double mutant enzymes generally showed little changes in substrate and cofactor binding but synergistic decreases in forward hydride transfer rates, while the decreases in reverse rates were additive. Along with supporting information from mixed quantum/classical MD simulations [Agarwal, P. K., Billeter, S. R., Rajagopalan, P. T., Benkovic, S. J., and Hammes-Schiffer, S. (2002) *Proc. Natl. Acad. Sci. U.S.A. 99*, 2794−2799], the data suggest that a coupled dynamic motion of these distal residues enhances crossing of the chemical reaction barrier and imply an expanded nonstatic role for the protein fold in catalysis.

The role of coupled protein motions in enzymic catalysis has recently attracted considerable attention (*4*−*6*). In addition to the orchestrated interactions of substrates and active site residues that accompany progress along the reaction coordinate, the participation of residues distal to the active site has also been proposed to augment enzyme catalysis. Protein motions are also crucial in achieving preorganization of enzyme active sites and transition-state stabilization. Dihydrofolate reductase (DHFR)[1] is a paradigm in which the role of dynamics in catalysis continues to be revealed by a combination of kinetic, structural, and computational studies.

Dihydrofolate reductase (DHFR, EC 1.5.1.3) is an essential enzyme required for normal folate metabolism in prokaryotes and eukaryotes and maintains tetrahydrofolate levels needed to support the biosynthesis of purines, pyrimidines, and amino acids. DHFR catalyzes the stereospecific reduction of 7,8-dihydrofolate (H_2F) to 5,6,7,8-tetrahydrofolate (H_4F), using nicotinamide adenine dinucleotide phosphate (NADPH) as the cofactor. Specifically, the *pro-R* hydride is transferred from the C-4 of NADPH to C-6 of H_2F with concomitant protonation at N-5. The complete kinetic scheme for DHFR catalysis has been derived using a combination of equilibrium binding, steady-state kinetic, and transient-state kinetic experiments and correctly predicts the full-time course kinetics as a function of substrate concentrations and pH (*7*, *8*). A maximal rate of H_4F turnover involves cycling between five kinetically observable species with the slowest step being H_4F release from the reduced ternary complex (DHFR·NADPH·H_4F). Similar kinetic schemes were constructed for mutant enzymes, allowing precise analyses into the function of the mutated regions (*2*, *9*−*19*).

The structural features of DHFR facilitate passage through the aforementioned preferred catalytic pathway. *Escherichia coli* DHFR is a monomeric enzyme featuring an eight-stranded β-sheet (βA−βH) and four α-helices connected by flexible loop regions (Figure 1A). The three catalytically significant flexible loops are the Met-20 loop (residues 9−24), the βF−βG loop (residues 117−131), and the βG−βH loop (residues 146−148). A comparison of crystal structures representative of all five complexes as well as an approximation of the transition state (TS) in the preferred pathway has shown that the Met-20 loop adopts either a closed or an occluded conformation depending on the ligands

† This work was supported by NIH Grant GM24129 to S.J.B.

* Correspondence should be addressed to this author at the Department of Chemistry, The Pennsylvania State University, University Park, PA 16802. Telephone: (814) 865-2882, Fax: (814) 865-2973, E-mail: sjb1@psu.edu.

‡ Present address: Department of Chemistry, Emory University, 1515 Pierce Dr., Atlanta, GA 30322.

[1] Abbreviations: DHFR, dihydrofolate reductase; H_2F, 7,8-dihydrofolate; H_4F, 5,6,7,8-tetrahydrofolate; NADPH and NH, reduced nicotinamide adenine dinucleotide phosphate; DNADPH, 5,6-dihydro-NADPH; NADPD, [4′(*R*)-^{2}H]NADPH; $NADP^+$ and N^+, oxidized nicotinamide adenine dinucleotide phosphate; Mtx, methotrexate; DTT, dithiothreitol; TS, transition state; FRET, fluorescence resonance energy transfer.

10.1021/bi026369d CCC: $22.00
Published on Web 09/27/2002

bound (*20*). Motions of the Met-20 loop have been analyzed by 2D NOESY spectroscopy and revealed an oscillation frequency of 35 s^{-1}, similar to the off rate of H_4F, implying that loop movement may be a partially limiting step in substrate turnover (*21*). Substitution of residues 16−19 in the loop with a single glycine altered loop movement and decreased substrate binding 10-fold and hydride transfer 400-fold (*19, 21*).

In substrate analogue complexes (surrogates for DHFR·NADPH and DHFR·NADPH·H_2F), the Met-20 loop contacts NADPH through a closed state stabilized by hydrogen bonding of both Gly-15 and Glu-17 (Met-20 loop) with Asp-122 (βF−βG loop). The chemical reaction is accompanied by the disruption of these hydrogen bonds and formation of new ones between Asn-23 (Met-20 loop) and Ser-148 (βG−βH loop). Consequently, the Met-20 loop switches to the occluded state in the product complexes. The functions of the interloop interactions were verified by kinetic characterization of Asp-122 and Ser-148 mutant enzymes in which the hydrogen bonding ability was systematically perturbed (*9, 10*). The data suggested in particular that the interactions of Asp-122 lie along the reaction coordinate leading to the TS. Second, both Asp-122 and Ser-148 mutations altered ligand affinities, turnover, and the kinetically preferred pathway. Thus, the transitions between different conformational states characterized by Met-20 loop movement guide the reaction cycle.

Backbone and tryptophan side-chain dynamics of the ^{15}N-labeled DHFR·folate complex have also been studied and yielded residue-specific dynamic information (*22*). Four regions of enhanced flexibility indicating increased motions on the nanosecond to picosecond time scale included: (i) residues 16−22 in the Met-20 loop; (ii) residues 67−69 in the adenosine binding loop; (iii) residues 38 and 88 in the hinge regions; and (iv) residues 119−123 in the βF−βG loop. The DHFR·folate complex examined represented the product binary complex (DHFR·H_4F) with the Met-20 loop in the occluded state. Similar NMR studies included surrogate complexes of DHFR·DNADPH·folate and of DHFR·$NADP^+$·folate that represent the product ternary complexes (DHFR·$NADP^+$·H_4F and DHFR·NADPH·H_4F) and the Michaelis complex (DHFR·NADPH·H_2F), respectively (*23*). Many of the nanosecond to picosecond time scale backbone dynamics in the DHFR·folate and DHFR·DNADPH·folate complexes (Met-20 loop in the occluded state) were significantly damped in the DHFR·$NADP^+$·folate complex (Met-20 loop in the closed state). Molecular dynamics (MD) simulations performed on the same three ternary complexes showed correlated and anticorrelated motions involving spatially distinct regions in the DHFR structure in many of the same regions implicated in the dynamic NMR measurements (*24*).

The relationship between protein motions and catalysis suggested by the X-ray and NMR structural studies and computational methods was probed by site-directed mutagenesis of glycine-121, a highly mobile residue in the βF−βG loop residue that is ∼19 Å away from the reaction center (*2, 11*). The glycine-121 mutant enzymes showed weakened NADPH binding and dramatically slowed hydride transfer rates. The G121V mutant enzyme in particular had a 200-fold lower hydride transfer rate and featured an additional conformational change step in the Michaelis complex preceding the hydride transfer step (*2*). In general, mutations made in regions of correlated motions have a deleterious effect on DHFR activity and, in particular, the early portion of the kinetically preferred pathway. Significantly, MD simulations on the G121V mutant revealed an absence of similar patterns of correlated motion (C. L. Brooks, personal communication). In summary, there is evidence for coupling between backbone dynamics involving residues that are spatially well separated from the active site and the rate of hydride transfer, coupling that may lie along the reaction coordinate and promote crossing of the activation barrier.

Toward the broad goal of defining in greater detail the relationship between protein motions and the rate of hydride transfer, we sought to identify additional residues whose involvement in a coupled network may be required for efficient catalysis. We supplemented our above observations with a comprehensive sequence analysis of DHFR genomic data and found regions of conservation lining the active site as well as regions spatially removed from the active site. The collective analysis of (i) sequence conservation information, (ii) kinetic data for site-directed mutants, (iii) data from NMR spectroscopy for regions of dynamic motions, and (iv) MD simulations for correlated motions implicates a subset of residues (positions 15, 41−45, 60−63, 96−97, and 121−123) as possibly being involved in a coupled network. This paper focuses on the role of the distal yet tightly conserved region spanning residues 41−45 and its relation to residues 121−123. Specifically, site-directed mutagenesis of methionine-42 followed by kinetic characterization was carried out to probe its role in DHFR catalysis. We conclude that methionine-42 primarily functions in assisting hydride transfer. We then sought a linkage between positions 42 and 121 through double mutants that were found to display large nonadditive decreases in hydride transfer rates with little change in other kinetic parameters. Along with supporting computational evidence, these results suggest that the coupled motion of these and possibly other, yet unidentified residues constitutes a network that promotes barrier crossing and thereby increases the rate of hydride transfer. Such an evolutionarily conserved network of promoting motions implies an expanded role for the protein fold in enzyme catalysis.

MATERIALS AND METHODS

Sequence Conservation Analysis. The *Escherichia coli* DHFR protein sequence was first used to search for homologous protein sequences using the BLAST technique (*25*). A total of 36 homologous sequences (listed below) were used to create a preliminary alignment with Clustal-W (*26*). After refinement utilizing available structural data, the completed alignment was generated and the sequence conservation information mapped to the protein structure to produce Figure 1B. The programs MolScript and Raster3D were used to generate Figure 1 (*27*). The same sequence conservation patterns were later confirmed in a comprehensive alignment of 121 nonredundant and unique DHFR sequences that were obtained from SWISS−PROT and TrEMBL database searches. The following is a list of 36 species whose DHFR sequences were aligned: *Escherichia coli*, *Citrobacter freundii*, *Enterobacter aerogenes*, *Klebsiella aerogenes*, *Haemophilus influenzae*, *Salmonella typhimurium*, *Bacillus subtilis*, *Neisseria gonorrheae*, *Staphylococcus haemolyticus*, *Deinococcus radiodurans*, *Staphylococcus*

Table 1: Oligonucleotide Primers for Site-Directed Mutagenesis of the DHFR Gene[a]

primer	nucleotide sequence
DHFR-For	5′GCGGGATCCCATATGATCAGTCTGATTGCGGCG3′
DHFR-Rev	5′GCGTCTAGAGGATCCTTAACGACGCTCGAGGAT3′
M42F	5′CACCTTAAATAAACCCGTGATTTTTGGGCGCC-ATACCTGG3′
M42W	5′CCTTAAATAAACCCGTGATTTGGGGGCGCCAT-ACCTGG3′
G67V	5′AGTCAACCCGTGACCGATGA3′
G121A	5′CGATGCAGAAGTGGAAGCCGACACCCATTTTCCG3′
G121S	5′CGATGCAGAAGTGGAAAGCGACACCCATTTTCC3′
G121V	5′CGATGCAGAAGTGGAAGTCGACACCCATTTTCCG3′
F153S	5′GCATAGCTATTGTTCCGAAATCCTCGAGCGTC-GTTAAGGATCCTCTAGACGC3′

[a] Mutagenic reverse primers (not shown) were reverse-complements of the forward sequences. The underlined nucleotides indicate location of the mutations.

epidermidis, *Staphylococcus aureus*, *Streptococcus pneumoniae*, *Haloferax volcanii*, *Enterococcus faecium*, *Enterococcus faecalis*, *Mycobacterium tuberculosis*, *Mycobacterium avium*, *Zymomonas mobiliz*, *Aeromonas salmonicida*, *Lactococcus lactis*, *Lactobacillus casei*, *Heliothis virescens*, *Pneumocystis carinii*, *Chlamidia pneumoniae*, *Proteus mirabilis*, *Homo sapiens*, *Candida albicans*, *Herpesvirus saimiri*, *Aedes albopictus*, *Drosophila melanogaster*, *Chlamidia trachomatis*, *Caenorhabditis elegans*, *Mus musculus*, *Shigella sonnei*, and *Shigella flexneri*.

Materials. All reagents were purchased from Fisher Scientific (Pittsburgh, PA) or Sigma (St. Louis, MO). Propagation of plasmid DNA was carried out using *E. coli* DH5α cells. Restriction and DNA-modifying enzymes were purchased from New England Biolabs (Beverly, MA). Oligonucleotides for mutagenesis were synthesized on a 8909 Perceptive Biosystems Expedite DNA synthesizer. All assays were conducted in constant ionic strength MTEN buffer (50 mM MES, 25 mM Tris, 25 mM ethanolamine, and 100 mM sodium chloride), pH 5−10 at 25 °C.

Preparation of DHFR Ligands. 7,8-Dihydrofolate (H_2F) was prepared from folic acid by dithionite reduction (*28*). 5,6,7,8-(6*S*)-Tetrahydrofolate (H_4F) was prepared by the enzymatic reduction of H_2F using *E. coli* DHFR (*29*). NADPH and $NADP^+$ were purchased from Sigma. The deuterated cofactor analogue, [4′(*R*)-^{2}H]NADPH (NADPD), was prepared by using alcohol dehydrogenase from *Thermoanerobium brokii* and 2-propanol-d_8 to reduce $NADP^+$ (*30*). 5,6-Dihydro-NADPH (DNADPH) was synthesized and gifted by Dr. D. C. Wahnon (*9*). Concentrations of ligand solutions were calculated using the following extinction coefficients: 28 mM^{-1} cm^{-1} for H_2F at 282 nm and pH 7.4, 28 mM^{-1} cm^{-1} for H_4F at 297 nm and pH 7.5, 22.1 mM^{-1} cm^{-1} for methotrexate (Mtx) at 302 nm in 0.1 M KOH, 6.22 mM^{-1} cm^{-1} for NADPH (NADPD) at 340 nm and pH 7.0, 18 mM^{-1} cm^{-1} for $NADP^+$ at 259 nm and pH 7.0, and 18 mM^{-1} cm^{-1} for DNADPH at 259 nm and pH 7.0 (*9*).

Construction of Mutant DHFRs. All site-directed mutations were introduced by primer overlap extension. For single mutants, the expression plasmid pET22b-DHFR was used as template for the first amplification (*2*). Relevant primer sequences are listed in Table 1. In brief, two independent polymerase chain reactions (PCRs) were conducted for each construct; the first reaction with DHFR-For and mutagenic reverse primers, the second reaction with the mutagenic forward and DHFR-Rev primers. The resulting products were gel-purified and then used in a subsequent PCR, employing DHFR-For and DHFR-Rev primers. The desired expression construct was obtained by restriction digestion of the final product with *Nco*I and *Bam*HI, followed by ligation with the vector portion of the *Nco*I- and *Bam*HI-cleaved pET22b-DHFR. After transformation into the *E. coli* DH5α-E strain (Invitrogen, Carlsbad, CA) and preparation of plasmid DNA, the desired mutations were confirmed by DNA sequencing. For double mutants, the corresponding single mutant plasmid served as template for a second overlap extension experiment. Mutations at position 153 were introduced by substitution of the DHFR-Rev primer with the listed primer. For protein expression, the individual plasmids were recovered and transformed into the *E. coli* BL21(DE3) strain.

Purification of DHFR Mutant Enzymes. Wild-type and mutant DHFRs were purified as described previously (*9*). *E. coli* BL21(DE3) cells containing the pET22b-DHFR expression plasmid were grown at 37 °C to mid-log phase in 2 L of NCZYM medium containing 100 μg/mL ampicillin and induced with 0.5 mM isopropyl-β-D-thiogalactopyranoside (IPTG). After induction for 5 h at 37 °C, the cells were harvested by centrifugation. From this point on, all further purification procedures were carried out at 4 °C. The cell pellet was then resuspended in 100 mL of a 50 mM sodium phosphate, pH 7.0, buffer containing 500 mM sodium chloride, 1 mM ethylenediaminetetraacetate (EDTA), 1 mM dithiothreitol (DTT), 1% Triton X-100, 10% poly(ethylene glycol)-8000 (PEG-8000), 10 μg/mL trypsin inhibitor, 10 μg/mL leupeptin, 10 μg/mL pepstatin-A, and 100 μg/mL phenylmethanesulfonyl fluoride. Lysis was then initiated by adding 50 mg of lysozyme and completed by sonication. Centrifugation followed by ultracentrifugation yielded a clarified lysate, which was loaded onto a preequilibrated methotrexate−agarose column of 3 mL bed volume. Following extensive washing, the DHFR mutant protein was eluted with pH 9.5 buffer containing 5 mM folate. For a few mutant enzymes, weakened methotrexate binding caused lower yields and necessitated lower wash volumes. After methotrexate affinity purification and dialysis into low-salt buffer, the proteins were loaded onto a DE-52 column for anion-exchange purification to remove folate. After the column was washed, the bound DHFR was eluted using a 50−500 mM sodium chloride gradient. After concentration and dialysis to remove salt, the mutant proteins were quickly frozen in liquid nitrogen and stored at −80 °C. DHFR was quantified by both absorbance ($\epsilon_{280} = 74.6$ mM^{-1} cm^{-1}) and titration with methotrexate. All mutant enzymes thus isolated were purified to apparent homogeneity as judged by 15% SDS−PAGE analysis.

Thermodynamic Dissociation Constants. The equilibrium dissociation constants, K_D, for DHFR−ligand complexes were measured by the quenching of intrinsic protein fluorescence as a function of ligand concentration using a Fluoromax-2 spectrofluorometer (Jobin Yvon Inc., Edison, NJ). Typically, DHFR was added to filtered, degassed, and argon-saturated MTEN buffer at pH 7.0 in a fluorescence cuvette. Enzyme concentrations were kept below the K_D being measured and were typically 25−100 nM. Wild-type *E. coli* DHFR contains five tryptophan residues whose combined fluorescence was monitored at 340 nm with excitation at 290 nm. Enzyme fluorescence data were

collected as a function of added ligand. The data after inner filter effect corrections were fit to a hyperbolic equation to generate the K_D value. The extraordinarily tight binding of methotrexate to DHFR was used to accurately determine protein concentrations. The titration of DHFR with methotrexate was carried out at enzyme concentrations substantially higher than K_D. Under these conditions, a monotonic decrease in enzyme fluorescence is observed until the active site is saturated. Fitting the data yields the concentration of DHFR active sites. All the binding experiments were performed at room temperature in MTEN buffer, pH 7.0.

Steady-State Kinetics. Maximal rates of substrate turnover were recorded with saturating amounts of substrate and cofactor by monitoring the decrease in reaction absorbance at 340 nm ($\Delta\epsilon_{340} = 13.2\ mM^{-1}\ cm^{-1}$) using a Cary 1E UV−Vis spectrophotometer (Varian Inc., Palo Alto, CA). All assays were conducted at 25 °C employing a water-jacketed cuvette holder. Typically, 10−1000 nM enzyme in degassed and argon-saturated MTEN buffer (pH 7.0 or 9.0) containing 1 mM DTT was preincubated with 100 μM cofactor to avoid hysteresis, and the reaction was initiated by adding 100 μM substrate. The resulting rate of absorbance decrease was typically 0.1 unit/min and could be measured conveniently and accurately. Substrate and cofactor concentrations were doubled to ensure that the reaction rate being measured was maximal, and the k_{cat} value was then calculated. Maximal reaction rates were likewise measured with 100 μM NADPD. The isotope effect ^DV ($^DV = k_H/k_D$) was then calculated.

For the reverse reaction involving oxidation of H_4F and production of NADPH, the rate of absorbance increase at 340 nm was measured. The extreme instability of H_4F necessitated precautions to minimize contact with oxygen, light, and temperatures greater than 4 °C (except during assays). All reverse rate measurements were carried out in MTEN buffer, pH 9.0, containing 5 mM DTT. In typical experiments, DHFR mutant enzymes (100 nM) were preincubated with 2 mM $NADP^+$, and the reactions were initiated by the addition of 100 μM H_4F. After measuring the rate of absorbance increase, the specific reverse rate was calculated. Identical reaction rates were observed on doubling H_4F and $NADP^+$ concentrations, ensuring conditions of saturation.

Transient-State Kinetics. All transient or pre-steady-state kinetic measurements were made on a stopped-flow instrument (Applied Photophysics Ltd., Leatherhead, U.K.). Kinetic studies of ligand binding, involving on- and off-rate measurements, were accomplished by following the ligand-dependent quenching of intrinsic enzyme fluorescence. Enzyme tryptophans were excited at 290 nm, and the resulting fluorescence was measured using a 305 nm cutoff filter. Rapid mixing with ligand generated a transient of decreasing fluorescence, which was usually fitted to a single-exponential function to give the observed rate. Association or on-rate (k_{on}) measurements were performed using the relaxation technique. Ligand dissociation rates were determined accurately by the method of competition. Table 2 lists the traps used to measure ligand off-rates from various DHFR complexes. Further details can be found under Results while the underlying principles behind the design of these experiments are discussed elsewhere (*7*).

The chemical reaction was monitored at the pre-steady-state level by taking advantage of the strong fluorescence resonance energy transfer (FRET) between DHFR and bound reduced cofactor. The protein (tryptophan) emission spectrum overlaps widely with the nicotinamide absorption spectrum. Consequently, when the enzyme−cofactor complex is excited at 290 nm, the FRET results in strong reduced cofactor fluorescence at 450 nm, which is observed through a 405 nm cutoff filter. Since $NADP^+$ is nonfluorescent, the chemical step can be followed by the loss of fluorescence. In a typical experiment, 3 μM DHFR was preincubated with a saturating amount of either NADPH or NADPD (100 μM) in MTEN buffer, pH 5−10 at 25 °C. The reaction was initiated by rapid mixing with H_2F (instrument-controlled). In addition to the fluorescence, absorbance data were also collected. The absorbance mode is substantially less sensitive, but is important in verifying the conclusions drawn from the fluorescence data. The use of NADPD as a cofactor allows for the unambiguous assignment of the chemical step by observing the expected isotope effect ($^DV = 2.8-3.0$). The hydride transfer rates measured varied substantially from the wild-type rate of 228 s^{-1} and necessitated both multiple and single turnover experiments which are discussed at length under Results.

Table 2: Measurement of Ligand Dissociation Rates (k_{off}) by Competition at 25 °C in MTEN Buffer, pH 7.0

ligand	enzyme species	trap
NADPH	DHFR·NADPH	$NADP^+$
	DHFR·H_4F·NADPH	
	DHFR·folate·NADPH	
$NADP^+$	DHFR·$NADP^+$	NADPH
	DHFR·H_4F·$NADP^+$	
	DHFR·H_2F·$NADP^+$	
H_2F	DHFR·H_2F	Mtx
	DHFR·H_2F·DNADPH	
	DHFR·H_2F·$NADP^+$	
H_4F	DHFR·H_4F	Mtx
	DHFR·H_4F·NADPH	
	DHFR·H_4F·$NADP^+$	

RESULTS

Sequence Conservation, Structure, and Function Analysis. A comprehensive global alignment of 36 DHFR protein sequences was prepared as described in the previous section. The resulting information was mapped to the *E. coli* DHFR structure to generate Figure 1B. The figure permits easy visualization of the conserved regions, namely, positions 7, 14−15, 21−22, 27, 31, 35, 40−43, 44, 46, 54, 61−63, 95−96, 100, 113, and 121−122. Conservation of most residues can be explained readily by their previously established roles in DHFR catalysis obtained by site-directed mutagenesis and kinetic characterization. The functions are summarized as follows. Residues 7, 14, 15, 21, 31, 35, 44, 46, 54, and 100 either line the active site and/or contact substrate or cofactor (*8*). Hydrogen bonding to the substrate in the active site involves tryptophan-22, aspartate-27, and threonine-113 (*8*, *14*). Structurally, the cis peptide bond geometry between positions 95 and 96 requires glycines. Aspartate-122 in the βF−βG loop forms a functionally important hydrogen bond with the Met-20 loop in the closed state (*10*). Adjacent to aspartate-122 is the moderately conserved and highly motional glycine-121, which primarily influences the hydride transfer step (*2*). In contrast, the tight sequence conservation of the distal residues 40−43 and 61−63 (VIMG for residues 40−43, and ILS for residues 61−63) cannot be reconciled

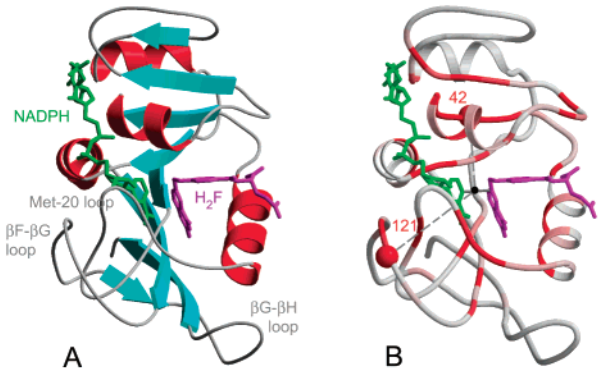

FIGURE 1: (A) Structure of *E. coli* DHFR. Secondary structure elements and substrate (H_2F, purple) and cofactor (NADPH, green) structures are shown. The three catalytically important and flexible loop structures are also indicated. (B) Sequence conservation information mapped to the *E. coli* DHFR structure. The C_α trace is gradient-colored on a scale of gray (least conserved) to red (most conserved). The location of residues methionine-42 and glycine-121 (red spheres) relative to the transferring hydride (black sphere) is displayed. Both (A) and (B) were generated from PDB coordinates 1rx2 where the Met-20 loop adopts the closed conformation.

with any obvious function. Both regions (40−43 and 61−63) are part of the β-sheet structure and likely contribute to maintaining a structurally important hydrophobic core. MD simulations reveal strong anti-correlated motions of both regions with glycine-121 and suggest a possible role in assisting hydride transfer as the rationale for conservation (*24*). On this basis, appropriate single and double mutant enzymes were created and studied to measure the effect of the amino acid changes on the rates of hydride transfer and other steps.

Isolation and Structural Properties of DHFR Mutant Enzymes. The mutant enzymes were expressed using a pET22b-derived plasmid and purified to homogeneity using previously developed procedures (*2*, *9*). Typically, 1−5 mg of purified protein per liter of culture was obtained. The comparable ability of the mutant enzymes in binding methotrexate, substrate, and cofactor and their similar circular dichroism spectra relative to wild-type DHFR (data not shown) suggest no gross perturbation in the overall enzyme structure.

Thermodynamic Binding of Ligands. The thermodynamic dissociation constants (K_D) for substrate and cofactor binding to all mutant enzymes were measured using quenching of the intrinsic enzyme fluorescence as described under Materials and Methods and are summarized in Table 3. All substrate dissociation constant values were in the range of 0.10−0.82 μM, which is approximately 3-fold lower and higher than the wild-type value of 0.33 μM. Mutations of Met-42 produced no effect on NADPH binding while mutations of Gly-121 weakened NADPH binding up to a maximum of 40-fold for G121V, as previously noted (*2*). NADPH binding improved slightly for the Met-42-Gly-121 double mutants relative to the Gly-121 single mutants with the exception of M42F-G121S. Dissociation constants for H_4F and $NADP^+$ binding were measured for M42F, M42W, G121S, M42F-G121S, and M42W-G121S mutant DHFRs and are listed in Table 4. Unexpectedly, the M42F and M42W mutations attenuated H_4F binding by approximately 13-fold. The G121S mutation suppressed this effect as evidenced by the lower dissociation constants for the double mutant enzymes. $NADP^+$ binding was destabilized 2−3-fold by both Met-42 and Gly-121 single mutations. The effects combine in the double mutants to further slightly weaken $NADP^+$ binding. Summarizing, the overall effects of the mutations studied on reactant and product binding were relatively small (less than 1 kcal/mol) and followed no discernible trend.

Table 3: Equilibrium Thermodynamic Dissociation Constants for Enzyme−Substrate and Enzyme−Cofactor Complexes at 25 °C in MTEN Buffer, pH 7.0

DHFR	H_2F	NADPH
WT	0.33 ± 0.06	0.34 ± 0.08
M42F	0.25 ± 0.05	0.22 ± 0.04
M42W	0.43 ± 0.1	0.27 ± 0.03
G67V (*12*)	0.21 ± 0.02	1.0 ± 0.1
G121S	0.39 ± 0.05	3.2 ± 0.4
G121V	0.36 ± 0.02	14.2 ± 0.8
M42W-G67V	0.10 ± 0.02	0.78 ± 0.15
M42F-G121A	0.26 ± 0.05	0.82 ± 0.18
M42F-G121S	0.82 ± 0.17	11 ± 3
M42W-G121A	0.14 ± 0.02	1.2 ± 0.3
M42W-G121S	0.18 ± 0.03	2.3 ± 0.4
M42W-G121V	0.15 ± 0.03	6.7 ± 1.4
G67V-G121S	0.40 ± 0.05	0.71 ± 0.14
G121S-F153S	0.21 ± 0.02	1.3 ± 0.2

Table 4: Equilibrium Thermodynamic Dissociation Constants for Enzyme−Product Complexes at 25 °C in MTEN Buffer, pH 7.0

DHFR	H_4F	$NADP^+$
WT	0.13 ± 0.03	23 ± 4
M42F	1.6 ± 0.3	53 ± 9
M42W	1.7 ± 0.2	72 ± 9
G121S	0.16 ± 0.02	46 ± 3
M42F-G121S	0.50 ± 0.08	60 ± 11
M42W-G121S	0.12 ± 0.02	88 ± 10

Kinetics of Ligand Binding. Ligand-dependent quenching of intrinsic DHFR fluorescence was followed by stopped-flow techniques to study the kinetics of ligand binding (*7*). The relaxation method was utilized to measure the association rates for the binding of H_2F, H_4F, NADPH, and $NADP^+$ to M42W DHFR. The fluorescence transient obtained by mixing ligand and free enzyme was fit appropriately (typically, a single-exponential fit) to evaluate the first-order rate constant (k_{obs}) with which the system approached equilibrium. k_{obs} is related to the association rate constant (k_{on}), the dissociation rate constant (k_{off}), and ligand concentration ([L]) by the equation: $k_{obs} = k_{on}[L] + k_{off}$. The k_{obs} values were recorded at different [L] values and plotted where the slope and intercept of the resulting line were k_{on} and k_{off}, respectively.

Ligand dissociation rates (k_{off}) from all possible complexes were measured more accurately by the competition method, which takes advantage of the difference between the fluorescence end points for two ligands. Table 2 summarizes the traps used for the ligands whose dissociation rates were being measured. Methotrexate, a tight binding anti-folate compound, served as the trap in the measurement of all H_2F and H_4F dissociation rates. NADPH and $NADP^+$ were traps in the measurement of each other's dissociation rates. Experimentally, the enzyme complex (E·L in Scheme 1) was rapidly mixed with excess trap ligand (T). Under the conditions $k_1[L] \ll k_2[T] \gg k_{-1}$, dissociation of ligand L ($k_{-1} = k_{off}$) is rate-limiting and can be obtained accurately.

Scheme 1: Ligand Off-Rates

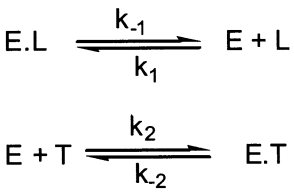

Scheme 2: Kinetic Scheme for M42W DHFR at 25 °C in MTEN Buffer, pH 7.0[a]

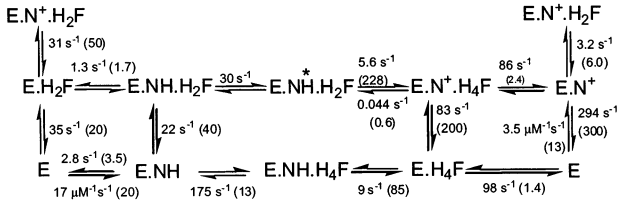

[a] Abbreviations: NH, NADPH; N^+, $NADP^+$; H_2F, dihydrofolate; H_4F, tetrahydrofolate. Respective wild-type DHFR values are indicated in parentheses.

This condition was affirmed by the trap concentration independent nature of the measured rate. The dissociation rates from the reactive ternary complex (complex with H_2F and NADPH) were approximated using nonreactive substrate and cofactor analogues. The surrogate ternary complex with folate and NADPH with $NADP^+$ acting as the trapping reagent provided an estimate of the NADPH dissociation rate from the DHFR·NADPH·H_2F complex. Similarly, the complex with H_2F and DNADPH (5,6-dihydro-NADPH) served to estimate the H_2F dissociation rate from the DHFR·NADPH·H_2F species.

The association, dissociation, and hydride transfer rates for M42W DHFR are summarized in Scheme 2, which predicts the time course of catalysis at 25 °C and pH 7.0. The association rate of NADPH (17 μM^{-1} s^{-1}) showed little change from the wild-type value of 20 μM^{-1} s^{-1}. The oxidized cofactor, $NADP^+$, association rate was reduced 4-fold. The association rates for H_2F and H_4F binding could not be determined due to insufficient signal intensity and high dissociation rate, respectively. $NADP^+$ dissociation rates showed little deviation from wild-type values with a maximum 2.5-fold reduction for the rate from the product ternary complex (E·N^+·H_4F in Scheme 2). NADPH dissociation rates were unperturbed relative to wild-type DHFR with the exception of the reduced ternary complex (E·NH·H_4F in Scheme 2) where there was a 10-fold reduction. The H_2F dissociation rate from the binary complex (E·H_2F) was raised 1.7-fold, while the rates from both ternary complexes (E·N^+·H_2F and E·NH·H_2F) were lowered less than 2-fold.

In contrast to the unaffected H_2F dissociation rates, the H_4F dissociation rates were significantly perturbed from the wild-type values. H_4F dissociation from the binary complex was 70-fold faster than wild-type DHFR, while dissociation from the product ternary complex (E·N^+·H_4F) and the reduced ternary complex (E·NH·H_4F) was raised 36- and 13-fold, respectively. The increase in H_4F dissociation rate primarily accounts for the higher thermodynamic dissociation constant (Table 4). Moreover, the NADPH and H_4F dissociation rates were highest in the reduced ternary complex. This indicates that the antagonistic negative cooperativity observed in the wild-type enzyme, resulting from the presence of both reduced species, is at least partially retained in the M42W enzyme. Partitioning of the immediate ternary product complex, however, directs a greater flux toward dissociation of H_4F from the binary rather than mixed ternary complexes relative to wild-type DHFR.

Steady-State Kinetics. The steady-state rates (k_{cat}) in the forward direction were determined as described under Materials and Methods. They were assessed for all mutant enzymes at pH 7.0 and 9.0, and at saturating substrate (H_2F) and cofactor (NADPH or NADPD) concentrations. The primary isotope effects (^DV) were then calculated. For the wild-type enzyme at pH 7.0, k_{cat} is controlled by H_4F dissociation from the reduced ternary complex (E·NH·H_4F in Scheme 2), resulting in no isotope effect being observed ($^DV = 1.0$) (*7*). However, at pH 9.0, hydride transfer becomes rate-limiting and the theoretically predicted maximum isotope effect ($^DV = 2.8-3.0$) is fully expressed. The isotope effect values were thus used to judge the contribution of the hydride transfer (chemical reaction) step to the overall reaction rate. With the exception of the M42F enzyme, all Met-42 and Gly-121 mutant DHFRs studied showed partial to complete expression of the isotope effect in k_{cat} ($^DV = 1.5-3.0$) at pH 7.0. Hence, the k_{cat} values provided an estimate of the rate constant for hydride transfer (k_{hyd}), which proved useful in planning the appropriate transient-state kinetic method to accurately measure k_{hyd}.

Kinetics of Hydride Transfer. Stopped-flow FRET and absorbance techniques were utilized to measure the rate constants of forward hydride transfer for all mutant enzymes as outlined under Materials and Methods. The absorbance mode data reflect NADPH levels and hence follow reaction chemistry only. In contrast, the FRET process between DHFR and NADPH depends on distance and environment. Thus, the fluorescence mode data report on conformational changes that affect the FRET process in addition to the chemical reaction where the FRET signal is lost. The rates of hydride transfer and preceding conformational changes were assessed by multiple and single turnover experiments as follows.

Multiple turnover experiments were used to measure hydride transfer rates of similar magnitude to wild-type DHFR (for example, M42F DHFR). Typically, a limiting amount of enzyme was first preincubated with excess cofactor (NADPH or NADPD) and then mixed with excess H_2F. For the wild-type and M42F mutant enzymes, the hydride transfer step was detected as a burst in the pre-steady-state. The anticipated burst amplitude in the absorbance mode (absorbance decrease calculated for one turnover) was verified. The assignment was confirmed by observing the complete primary kinetic isotope effect ($^DV = 2.8-3.0$) in the burst rate. In such cases, the burst rate equalled the rate constant for hydride transfer and was determined to be 228 and 159 s^{-1} for the wild-type and M42F DHFRs, respectively (Table 5).

Figure 2 describes the results of the multiple turnover experiment for M42W DHFR. In this case too, an apparent pre-steady-state burst was observed with a rate of 31 s^{-1}. However, no isotope effect or dependence on substrate and cofactor concentrations was noticed. Doubling the M42W DHFR concentration doubled the burst amplitude with no change in the burst rate. The same experiment in the absorbance mode revealed a 40 ms lag in product formation

Table 5: Forward Hydride Transfer Rates (k_{hyd}) at 25 °C in MTEN Buffer, pH 7.0

DHFR	k_{hyd} (s^{-1})	k_{hyd}(WT/mutant)
WT	228 ± 8	1.0
M42F	159 ± 17	1.4
M42W	5.6 ± 0.4 (31)[a]	41
G121A	38 ± 3	6.0
G121S	3.7 ± 0.4	62
G121V	1.4 ± 0.2 (3.5)	163
G67V (*12*)	190 ± 15	1.2
M42W-G67V	3.9 ± 0.4 (65)	59
M42F-G121A	1.3 ± 0.2	175
M42F-G121S	0.46 ± 0.08	496
M42W-G121A	0.27 ± 0.04 (0.60)	844
M42W-G121S	0.07 ± 0.01 (0.64)	3257
M42W-G121V	0.030 ± 0.005 (0.50)	7600
G67V-G121S	2.7 ± 0.2	84

[a] Rate constants for a conformational change step preceding hydride transfer are indicated in parentheses.

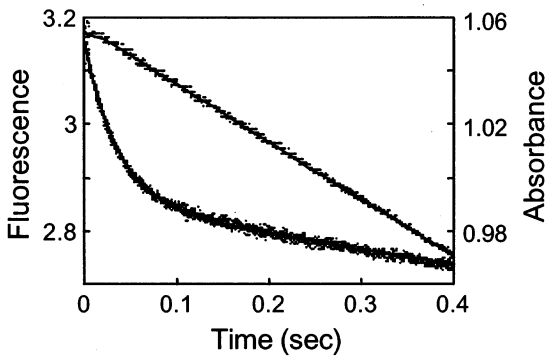

FIGURE 2: Time course of the hydride transfer process catalyzed by M42W DHFR, monitored by stopped-flow fluorescence resonance energy transfer (left axis) and absorbance (right axis). M42W DHFR (6 μM) was preincubated with 200 μM NADPH or NADPD and the reaction initiated by the addition of 200 μM H_2F. The final reaction concentrations were 3, 100, and 100 μM for enzyme, cofactor, and substrate, respectively. The solid line represents a fit of the fluorescence data to a single-exponential decay while the absorbance data points are not fitted but traced through smoothly.

followed by a steady-state rate (Figure 2). This steady-state rate was also found to show a partial isotope effect of 2.0 (data not shown). The evidence thus collectively implicates a zero-order conformational change step (rate of 31 s^{-1}) in M42W DHFR catalysis that precedes hydride transfer. Because the hydride transfer step only partially contributes to the overall steady-state rates in the M42W, G121S, and all double mutant enzymes, single turnover experiments were required to measure the rates accurately.

In a typical single turnover experiment, excess DHFR was preincubated with limiting amounts of cofactor (NADPH or NADPD) and then mixed with excess substrate. Consequently, the rate of the step that limits the conversion of H_2F to H_4F was measured. Figure 3 illustrates the experiment using the M42W-G121S enzyme as an example. Under the conditions described, the fluorescence datum revealed a two-step process and was fit to a double exponential function (Figure 3A). When NADPH was used, the first transient with the small positive amplitude occurred at a rate of 0.64 s^{-1}, while the second transient with the large negative amplitude had a rate of 0.07 s^{-1}. The same experiment when performed with NADPD clearly showed the absence and presence of an isotope effect for the first and second transients, respectively. The full expression of the isotope effect in the second transient unambiguously identifies it as the hydride transfer step. The positive amplitude of the first step suggests that the observed increase in cofactor fluorescence likely results from a conformational change. This was supported by the concentration-independent behavior of the rate. The amplitude in the absorbance mode confirmed that all the bound cofactor was oxidized (Figure 3B). In other experiments, the order of addition was changed by preincubating excess enzyme with limiting amounts of H_2F and mixing with excess cofactor. Similar rates were observed, implying no significant contribution from ligand dissociation was made to the overall rate being measured. The hydride transfer rates of all the mutant enzymes were determined likewise and are summarized in Table 5.

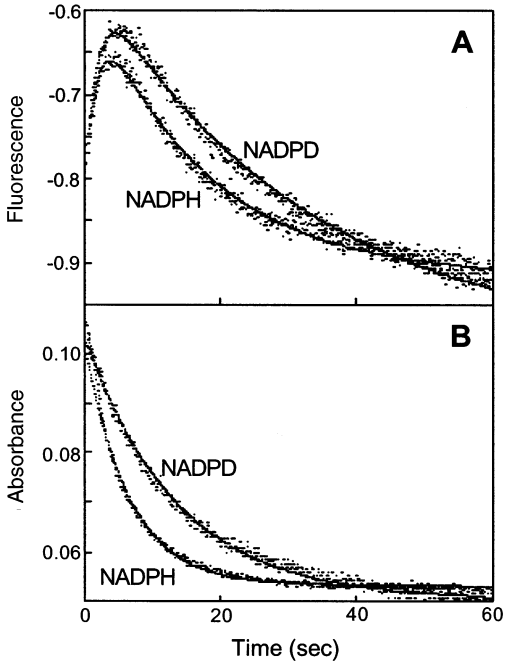

FIGURE 3: Measurement of the hydride transfer rate of M42W-G121S DHFR by single turnover experiments. M42W-G121S DHFR was preincubated with NADPH or NADPD and the reaction initiated by the addition of H_2F. The final concentrations were 33 μM for M42W-G121S DHFR, 2.2 μM for cofactor, and 100 μM for substrate. The reactions were monitored by (A) stopped-flow fluorescence resonance energy transfer and (B) stopped-flow absorbance techniques. The solid lines represent the fit of the data to (A) double and (B) single exponential functions.

The pH dependence of the forward hydride transfer rate in the range pH 6−10 was studied for representative single and double mutant DHFRs. The observed rate (k_{hyd}) vs pH data were plotted and fitted to the equation: $k_{hyd} = k_{max}/\{1 + K_A/[H^+]\}$ to obtain the pK_A of the enzyme ternary complex and the maximal rate (k_{max}) (*7*). The pK_A values do not deviate significantly from the wild-type value of 6.5 within experimental error (Table 6).

Analysis of Hydride Transfer Rates. Since both Met-42 and Gly-121 mutations have a deleterious influence on hydride transfer, double mutant enzymes were constructed and analyzed to probe for cooperative interactions between the two positions. A double mutational analysis method was utilized as follows (Scheme 3) (*31*). The effect on hydride transfer was first calculated for all mutant enzymes in free energy terms (eqs 3a−3c in Scheme 3). The terms $\Delta\Delta G_{42}$

Table 6: pH Dependence of Forward Hydride Transfer Rates at 25 °C

DHFR	pK_a
WT (*7*)	6.5
WT	6.6 ± 0.3
M42W	6.8 ± 0.3
G121S	6.3 ± 0.4
G121V	6.3 ± 0.3
M42W-G121S	6.3 ± 0.4
M42W-G121V	6.4 ± 0.4

Scheme 3: Analysis of Double Mutations

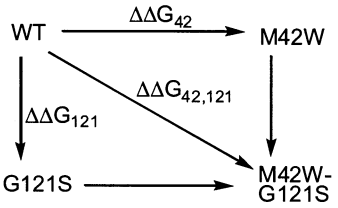

$$\Delta\Delta G_{42} = RT\ln(k_{WT}/k_{42}) \quad (3a)$$

$$\Delta\Delta G_{121} = RT\ln(k_{WT}/k_{121}) \quad (3b)$$

$$\Delta\Delta G_{42,121} = RT\ln(k_{WT}/k_{42,121}) \quad (3c)$$

$$\Delta G_I = \Delta\Delta G_{42,121} - (\Delta\Delta G_{42} + \Delta\Delta G_{121}) \quad (3d)$$

and $\Delta\Delta G_{121}$ reflect the changes in hydride transfer for individual mutations at positions 42 and 121, while $\Delta\Delta G_{42,121}$ expresses the effect in the double mutant enzyme. Each of these terms were calculated from the ratios of hydride transfer rates (Table 5). Equation 3d was then used to examine possible coupling between Met-42 and Gly-121 as follows: a coupling energy ΔG_I was computed for the five double mutant enzymes that involve positions 42 and 121. If the sites function independently, then the effect on the double mutant enzyme would be governed by the sum of the individual mutational effects and $\Delta G_I \sim 0$. Previous studies on other enzymes have shown that in most cases such additive behavior is observed if the sites of mutation are widely separated (*31*). All the ΔG_I values were positive, indicating that the Met-42 and Gly-121 mutations combined in a synergistic fashion to reduce the hydride transfer rate more than that predicted by an additive decrease. The coupling energies (ΔG_I) were plotted against the sum of the single mutant perturbations ($\Delta\Delta G_{42} + \Delta\Delta G_{121}$) to generate Figure 4. The plot shows clearly that the greatest synergy was seen for the M42F-G121A DHFR where the summed effect on $\Delta\Delta G$ of the single mutations was the least. The decrease in coupling energy parallels the decline in absolute values of the hydride transfer rates. Moreover, the near 10^4-fold decrease for the M42W-G121V DHFR was additive within experimental error. The uniqueness of such coupling interactions was tested by characterizing other double mutant enzymes and repeating the above analysis (Scheme 3). Mutations were made at Gly-67, which is a highly motional residue in the adenosine binding domain. The analysis showed that double mutations of Gly-67 with either Met-42 or Gly-121 caused strictly additive changes. Similar studies involving Ile-61 and Phe-153 mutations also showed non-additive decreases in hydride transfer rates.

Reverse Reaction Rates. For the wild-type DHFR, the considerably reduced forward hydride transfer rate at pH 9.0 permitted the determination of the reverse hydride transfer rate (*7*). Likewise, the lowered forward rates (k_{hyd} in Table 5) of the mutant DHFRs allowed the reverse rates to be measured, albeit with significantly increased error. The rates at pH 9.0 for select mutant enzymes are listed in Table 7. All the reverse rates were reduced in parallel with the decrease in forward rates. The M42F-G121S mutant DHFR showed a 518-fold decrease, which was largely accounted for by the combined effect of the individual mutations (2.2 × 194 = 427). Similarly, the 1493-fold decrease in the M42W-G121S enzyme was close to the expected decrease based on the combination of the individual mutations (6.7 × 194 = 1300). Hence, the effect on reverse rates using the previously outlined double mutational analysis is additive within experimental error.

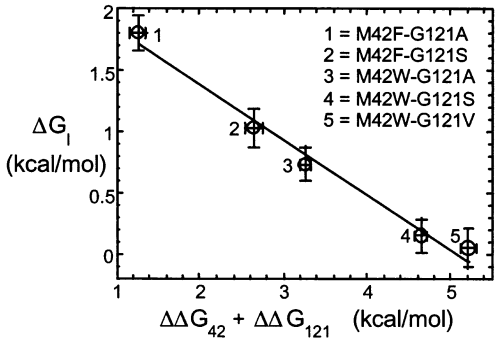

FIGURE 4: Nonadditive decrease in forward hydride transfer rates for double mutants of Met-42 and Gly-121. The abcissa term ($\Delta\Delta G_{42} + \Delta\Delta G_{121}$) is the sum of the effect of the individual mutations expressed in free energy terms, as described in Scheme 3. The ordinate term (ΔG_I) reflects the nonadditivity in the decrease of hydride transfer rates and is calculated using eq 3d in Scheme 3.

Table 7: Reverse Hydride Transfer Rates at 25 °C in MTEN Buffer, pH 9.0

DHFR	k_{hyd} (s^{-1})	k_{hyd}(WT/mutant)
WT	0.60 ± 0.05	1.0
M42F	0.27 ± 0.03	2.2
M42W	0.09 ± 0.02	6.7
G121S	(3.1 ± 0.5) × 10^{-3}	194
M42F-G121S	(1.9 ± 0.4) × 10^{-3}	518
M42W-G121S	(6.7 ± 2.1) × 10^{-4}	1493

DISCUSSION

DHFR exhibits functionally important dynamic motions on different time scales. The slower millisecond time scale subdomain motions such as Met-20 loop oscillations enhance catalysis by regulating passage through the kinetically preferred pathway (*19, 21*). The faster nanosecond−picosecond time scale dynamics observed for the βF−βG loop (Met-20 loop in the occluded state) are important for hydride transfer as demonstrated by mutagenesis of Gly-121(*2, 22, 23*). MD simulations have also underscored the significance of these correlated motions, which are unique to the Michaelis complex (DHFR·H_2F·NADPH) (*24*). Many of the amino acids in these regions of dynamic motion and in portions of the active site are strictly conserved in the sequence analysis reported here.

While the majority of conserved residues have been studied by site-specific mutagenesis (*2, 9*−*11, 13, 14, 16*−

18, 32−*34*), the roles of residues 40−43 and 61−63 in DHFR catalysis are not obvious. The correlated motion between Met-42 and Gly-121 seen in the MD simulations suggests a link to the hydride transfer step (*24*). The M42W mutation confirmed this connection by reducing the rate constant for hydride transfer 41-fold. Methionine-42 is distal to the active site and does not contact either substrate or cofactor directly, thereby decreasing the likelihood of any significant perturbation to ligand binding. The binding data (Tables 3 and 4) and the catalytic scheme (Scheme 2) for M42W DHFR catalysis largely support this notion. Indeed, cofactor binding was unaffected in Met-42 single mutant enzymes while the weakened binding of the double mutant enzymes likely resulted from the Gly-121 mutation as previously noted (*2*). $NADP^+$ binding was relatively unaltered as judged by both thermodynamic dissociation constants and dissociation rates. Given the unchanged H_2F binding, the reason for elevation of H_4F dissociation rates and dissociation constants is not clear, especially since the binding was restored in the double mutants.

Under saturating conditions of substrate and cofactor, the wild-type DHFR preferentially loses $NADP^+$ after reaction chemistry. This is followed by NADPH binding and then H_4F release, thereby leading to efficient cycling through the central pathway (*7*). For M42W DHFR, the H_4F dissociation rates from the binary and product ternary complexes are raised 70- and 36-fold, respectively. As a result, branching of the catalytic cycle to the right side in Scheme 2 is promoted, and significant amounts of free enzyme are likely formed. NADPH and H_2F then likely bind for another round of turnover. Tracing the pathway for maximal M42W DHFR catalyzed turnover, it is clear that hydride transfer is the slowest step and is likely rate-limiting. This is supported by a partial isotope effect of 2.2 in the steady-state rate at pH 7.0 with saturating substrate and cofactor concentrations. Additionally, a key feature of catalysis in the wild-type enzyme is the destabilizing influence of NADPH and H_4F on each other's binding in the reduced ternary complex ($E{\cdot}NH{\cdot}H_4F$ in Scheme 2). This results in a 50-fold elevation in NADPH dissociation rate relative to the reactive ternary complex, while the H_4F dissociation is 10 times faster relative to the $E{\cdot}H_4F$ binary complex (*7*). For M42W DHFR, similar analysis showed the same factors to be 7 for NADPH dissociation and 2 for H_4F dissociation. Thus, the M42W mutation caused the catalytically advantageous negative cooperativity to be weakened considerably.

The kinetically significant conformational change step preceding chemistry in M42W DHFR catalysis resembles that previously observed for Gly-121 mutant enzymes (*2*). Taking the experimental design and controls into account, the conformational change must involve a reorganization of the cofactor and/or enzyme structure that generates the reactive Michaelis complex. Such conformational change steps have been noted in horse liver alcohol dehydrogenase as well as mouse and human DHFRs (*35, 36*). Further, NMR evidence has shown that a similar step probably occurs in the wild-type *E. coli* DHFR at a rate $>2000\ s^{-1}$ and involves insertion of the nicotinamide moiety into the binding pocket (*23*). This high rate is beyond the detection range of conventional stopped-flow techniques and accounts for its absence in the kinetic scheme constructed (*7*). Both Met-42 and Gly-121 mutations slow this step, resulting in its kinetic manifestation. Further, these rates for the Met-42 and Gly-121 single and double mutant enzymes declined in parallel with the hydride transfer rate. Thus, the distal residue mutations studied likely affect dynamic properties that are crucial both to preorganization of the reactants to the Michaelis complex and in surmounting the chemical reaction barrier.

The decrease in forward hydride transfer rate toward high pH for wild-type DHFR is defined by the ionization of a single group ($pK_A = 6.5$) in the enzyme ternary complex (*7*). It is conceivable that the mutant DHFRs studied may have different loop dynamics and solvent accessibility to the active site interior, which could in turn alter the dielectric nature and the pH-dependent behavior. However, analysis of the pH vs rate data for select mutant enzymes showed little change in pK_A from the wild-type DHFR value. Thus, the observed marginal deviations in pK_A cannot account for the magnitude of rate decrease caused by the Met-42 and Gly-121 mutations.

Since both Met-42 and Gly-121 are important for hydride transfer, double mutational analysis was employed to examine if these distal residues were somehow coupled (*31*). By this approach, the effect of a second mutation on a mutant enzyme may be classified as additive, antagonistic, or synergistic with respect to the first mutation. Additive effects ($\Delta G_I \sim 0$ in Scheme 3) typically occur when noninteracting residues are mutated. When interacting residues are involved, the perturbation in the double mutant may be either lower (antagonistic, $\Delta G_I < 0$) or higher (synergistic, $\Delta G_I > 0$) than the sum effect of the individual mutations. The double mutational analysis method often cannot unambiguously interpret steady-state kinetic rate (k_{cat}) data due to changes in contributions from other steps. In contrast, microscopic rate constants measured by pre-steady-state kinetic methods, such as the hydride transfer rates reported here, facilitate clear interpretations. Further simplification is achieved due to similar pH-dependent behavior of the mutant enzymes (Table 6). Consequently, the pH 7 rates are related to the pH-independent rate values by similar proportionality constants and were used directly in the analysis.

The forward hydride transfer rates for the 42−121 double mutant series showed the greatest and the least synergistic decreases for M42F-G121A and M42W-G121V DHFRs, respectively. Such synergy could arise due to extensive unfolding, but was ruled out by the circular dichroism experiments and marginal binding changes. Further, a linear free energy relationship was established between the measure of synergy/nonadditivity (ΔG_I) and the sum effect in the parent single mutants ($\Delta\Delta G_{42} + \Delta\Delta G_{121}$). The abscissa spans a wide range of declining hydride transfer rates with a near 10^4-fold additive ($\Delta G_I \sim 0$) decrease for the M42W-G121V enzyme. Nonadditive mutational effects derived from changing four active site residues provided a DHFR where the forward hydride transfer rate was $0.12\ s^{-1}$ (*18*). Thus, it is conceivable that with an abrogation of promoting Met-42 and Gly-121 motions, the hydride transfer rate approaches a basal value for the DHFR scaffold, which primarily reflects the remaining preorganization contribution. The synergistic rate decrease may be viewed in terms of the increasing perturbation of the interactions that link Met-42 and Gly-121 through the protein structure, finally resulting in their uncoupling. Many such interresidue couplings likely exist,

and preliminary data suggest similar nonadditive decreases in hydride transfer rates for distal mutations of Ile-61 and Phe-153.[2] The highly conserved Ile-61 is located in the adenosine binding subdomain while Phe-153 is near the βG−βH loop and suppresses the negative effect of active site Asp-27 mutations (*1*). Because of the central importance of DHFR in cellular metabolism, changes in the hydride transfer rate appear to be buffered against deleterious mutations arising from environmental stress.

Additionally, mutations involving smaller amino acids (e.g., the M42A mutation, data not shown) displayed negligible changes from the wild-type rate. Mutations that result in higher hydride transfer rates are unlikely from an evolutionary perspective as there is little incentive given that the rate-limiting H_4F release step is 20 times slower. Double mutants of Gly-67 with either Met-42 or Gly-121 provided important experimental controls. Their additive behavior suggests that Gly-67 while being highly motional is not involved in the collective reaction coordinate. The distinction between such incidental (Gly-67) and important (Gly-121) dynamic motions may be drawn from the variation of dynamic NMR parameters between the closed and occluded conformational states. Specifically, the occluded state dynamics of Gly-121 are attenuated in the closed state, while the dynamics of Gly-67 are unchanged (*23*).

The reverse hydride transfer rates were also analyzed by the double mutational analysis method. Hydride transfer in both directions is strongly pH-dependent and is rate-limiting at pH 9.0 (*7*). This ensures that the steady-state rate measured for the reverse reaction accurately expresses the rate of reverse hydride transfer (maximal at pH 9.0). The participation of both Met-42 and Gly-121 in the reverse reaction was revealed by the decreased reverse rates of the mutants. Nevertheless, the combined rate decrease in the two double mutant enzymes studied was additive within experimental error. This lack of coupling in the reverse reaction is consistent with the absence of correlated motions in the product ternary complex (*24*). It also suggests that the effects of the mutations are not limited simply to the transition state. Thus, both residues may be visualized as promoting the reverse reaction but do so *independently*.

While the coupling of the distal Met-42 and Gly-121 residues and their roles in catalysis may be inferred from the kinetic data presented here, the physical nature of the process is not known. Intuitively, the rate decrease seemed linked with the increasing bulk of the amino acid substituent. Therefore, a likely explanation for the observed results may be the damping of promoting protein motions by the mutations. This is supported by recent mixed quantum/classical MD simulations of hydride transfer in which the real time trajectories depicted the time evolution of the donor−acceptor distance and the distance between residues Met-42 and Gly-121 (*3, 37*). The analysis implicated thermally averaged protein vibrations on the same time scale as the hydride transfer step, and revealed that the transition state was attained when both distances were minimal. In addition to affirming the participation of Met-42 and Gly-121, the study implicated faster time scale motions that cause oscillations in the slower millisecond domain that dominate the chemical process. Besides this pair of residues, others were identified (Ile-14, Phe-31, Tyr-100, etc.) as apparently belonging to a network of coupled motions.

Coupled motions may be studied experimentally by NMR methods. The NMR parameters of representative mutant enzyme complexes when compared with wild-type values should provide valuable information regarding altered coupled motions (*19, 21*). Changes in dynamics (reserved for changes in the TS theory pre-exponent term κ) are likely to impact quantum-mechanical hydrogen tunneling as well. The experimentally observed tunneling in the catalysis of hydride transfer reactions involves the hydride transferring through the chemical reaction barrier because of its wavelike property (*38*). Tunneling contributions to reaction rates are very sensitive to distances and consequently coupled motions. Preliminary experiments and computational results indicate that a significant tunneling contribution to the hydride transfer rate is likely in DHFR (*37*). It remains to be seen if the amino acid changes in the mutant enzymes affect tunneling.

A true quantitative measure of rate enhancement provided by the network of promoting motions may not be possible because of the inability to disentangle structure perturbation contributions inherent in mutagenesis techniques. Nevertheless, the consequence of interrupting this network is being simulated and will direct future site-directed mutagenesis studies. Incremental truncation based protein engineering methods are also being employed to generate functional hybrid enzymes from low homology DHFR sequences with the ultimate goal of defining how the coupling within the network is achieved. Such networks that invoke the participation of distal residues imply an expanded functional role of the protein fold and have been mapped in other systems (*39*). An appreciation of their contributions could be key to guiding future protein engineering efforts as well as understanding allosteric behavior, protein−protein interactions, and the action of drugs distal to the active site.

ACKNOWLEDGMENT

We thank Daphne C. Wahnon, Pratul K. Agarwal, and Prof. Sharon Hammes-Schiffer for useful discussions.

REFERENCES

1. Dion, A., Linn, C. E., Bradrick, T. D., Georghiou, S., and Howell, E. E. (1993) *Biochemistry 32*, 3479−3487.
2. Cameron, C. E., and Benkovic, S. J. (1997) *Biochemistry 36*, 15792−15800.
3. Agarwal, P. K., Billeter, S. R., Rajagopalan, P. T., Benkovic, S. J., and Hammes-Schiffer, S. (2002) *Proc. Natl. Acad. Sci. U.S.A. 99*, 2794−2799.
4. Berendsen, H. J., and Hayward, S. (2000) *Curr. Opin. Struct. Biol. 10*, 165−169.
5. Ishima, R., and Torchia, D. A. (2000) *Nat. Struct. Biol. 7*, 740−743.
6. Rajagopalan, P. T., and Benkovic, S. J. (2002) *Chem. Rec. 2*, 24−36.
7. Fierke, C. A., Johnson, K. A., and Benkovic, S. J. (1987) *Biochemistry 26*, 4085−4092.
8. Miller, G. P., and Benkovic, S. J. (1998) *Chem. Biol. 5*, R105−R113.
9. Miller, G. P., Wahnon, D. C., and Benkovic, S. J. (2001) *Biochemistry 40*, 867−875.
10. Miller, G. P., and Benkovic, S. J. (1998) *Biochemistry 37*, 6336−6342.
11. Miller, G. P., and Benkovic, S. J. (1998) *Biochemistry 37*, 6327−6335.

[2] The forward hydride transfer rates for F153S (*1*) and G121S-F153S are 242 ± 9 and 0.53 ± 0.08 s^{-1}, respectively (MTEN buffer, pH 7.0, 25 °C). ΔG_I was calculated to be 1.15 ± 0.16 kcal/mol.

12. Miller, G. P. (1997) Ph.D. Thesis, The Pennsylvania State University.
13. Adams, J. A., Fierke, C. A., and Benkovic, S. J. (1991) *Biochemistry 30*, 11046−11054.
14. Fierke, C. A., and Benkovic, S. J. (1989) *Biochemistry 28*, 478−486.
15. Benkovic, S. J., Fierke, C. A., and Naylor, A. M. (1988) *Science 239*, 1105−1110.
16. Mayer, R. J., Chen, J. T., Taira, K., Fierke, C. A., and Benkovic, S. J. (1986) *Proc. Natl. Acad. Sci. U.S.A. 83*, 7718−7720.
17. Wagner, C. R., Huang, Z., Singleton, S. F., and Benkovic, S. J. (1995) *Biochemistry 34*, 15671−15680.
18. Huang, Z., Wagner, C. R., and Benkovic, S. J. (1994) *Biochemistry 33*, 11576−11585.
19. Li, L., Falzone, C. J., Wright, P. E., and Benkovic, S. J. (1992) *Biochemistry 31*, 7826−7833.
20. Sawaya, M. R., and Kraut, J. (1997) *Biochemistry 36*, 586−603.
21. Falzone, C. J., Wright, P. E., and Benkovic, S. J. (1994) *Biochemistry 33*, 439−442.
22. Epstein, D. M., Benkovic, S. J., and Wright, P. E. (1995) *Biochemistry 34*, 11037−11048.
23. Osborne, M. J., Schnell, J., Benkovic, S. J., Dyson, H. J., and Wright, P. E. (2001) *Biochemistry 40*, 9846−9859.
24. Radkiewicz, J. L., and Brooks, C. L. (2000) *J. Am. Chem. Soc. 122*, 225−231.
25. Altschul, S. F., Gish, W., Miller, W., Myers, E. W., and Lipman, D. J. (1990) *J. Mol. Biol. 215*, 403−410.
26. Higgins, D. G., and Sharp, P. M. (1988) *Gene 73*, 237−244.
27. Kraulis, P. J. (1991) *J. Appl. Crystallogr. 24*, 946−950.
28. Blakley, R. L. (1960) *Nature 188*, 231−232.
29. Mathews, C. K., and Huennekens, F. M. (1960) *J. Biol. Chem. 235*, 3304−3308.
30. Jeong, S. S., and Gready, J. E. (1994) *Anal. Biochem. 221*, 273−277.
31. Mildvan, A. S., Weber, D. J., and Kuliopulos, A. (1992) *Arch. Biochem. Biophys. 294*, 327−340.
32. Chen, J. T., Taira, K., Tu, C. P., and Benkovic, S. J. (1987) *Biochemistry 26*, 4093−4100.
33. Murphy, D. J., and Benkovic, S. J. (1989) *Biochemistry 28*, 3025−3031.
34. Wagner, C. R., Thillet, J., and Benkovic, S. J. (1992) *Biochemistry 31*, 7834−7840.
35. Eklund, H., Samama, J. P., and Jones, T. A. (1984) *Biochemistry 23*, 5982−5996.
36. Beard, W. A., Appleman, J. R., Delcamp, T. J., Freisheim, J. H., and Blakley, R. L. (1989) *J. Biol. Chem. 264*, 9391−9399.
37. Agarwal, P. K., Billeter, S. R., and Hammes-Schiffer, S. (2002) *J. Phys. Chem. B 106*, 3283−3293.
38. Kohen, A., Cannio, R., Bartolucci, S., and Klinman, J. P. (1999) *Nature 399*, 496−499.
39. Lockless, S. W., and Ranganathan, R. (1999) *Science 286*, 295−299.

BI026369D